Wave transmission in Hostun sand: multiaxial experiments

Tarek Sadek,* Martin Lings,* Luiza Dihoru,* David Muir Wood*

Summary

Laboratory geophysical techniques using waves transmitted by piezoceramic elements have become popular for estimating the very small strain stiffness of soils. Piezoceramic Bender/Extender elements have been installed in a multiaxial cubical cell which is being used to study the multiaxial stiffness of dry Hostun sand. The elements can be used to track wave transmission in both shear and compression modes both across from one side to the opposite side of the cube and diagonally from one side to an adjacent side and thus to deduce the elements of the cross-anisotropic stiffness matrix of the sand. Practicalities of the bender installation reduce the degree of redundancy in these deductions. An assessment of the evolution of elastic anisotropy under axially symmetric stress conditions is presented.

Keywords: sand, multiaxial test, laboratory geophysics, anisotropy

Introduction

Most constitutive models include some description of elastic behaviour as a fundamental ingredient. The extent of the elastic region – described by a yield surface – may be small or even zero in an actual elastic-plastic model: evidence from discrete element analysis of particle assemblies suggests that more or less every perturbation will induce some slip at particle contacts and thus some inelastic deformation (for example, Zhang and Thornton 2006); but very sensitive experimental studies suggest that there may indeed be a finite strain region within which response is reversible and non-dissipative (for example, Hoque and Tatsuoka 2004) show non-hysteretic response in cycles of amplitude ±0.002% recorded using local deformation transducers for Ticino sand). However, there is at least a theoretical notion that for infinitesimal stress or strain excursions the response might be truly elastic and recoverable. The measurement of such elastic response requires a technique that imposes minimal disturbance to the soil so that it can be considered to reveal a 'constant fabric' or zero strain stiffness property. Static techniques have been used with very high resolution displacement measurement devices but it has been found simpler, in terms of the required equipment, to use laboratory geophysics and to determine the constant fabric stiffness from the speed of propagation of low amplitude waves through the soil, generated by means of piezoceramic elements.

It is known from laboratory testing that irrecoverable plastic strains are generated for quite small stress changes and such plastic strains are presumably associated with changes in the fabric of the soil. Discrete element modelling shows that even if the geometrical location of particles does not change the orientation of the more heavily loaded contacts between particles – the kinetic fabric – certainly does. As the fabric changes so the elastic stiffness properties are expected to change and the anisotropy of the fabric is likely to translate into anisotropy of stiffness. Thus this stiffness anisotropy is expected to evolve with stress history and it is found, for example, that the onset of localised shear deformation in sands is strongly influenced by the anisotropy of elastic stiffness [Gajo *et al.*, 2004]. It is consequently of practical relevance to conduct experiments in which the evolution of elastic anisotropy with stress history is explored.

Such evolution has previously been studied through conventional axially symmetric triaxial testing by means of piezoceramic elements inserted in the end platens and through the confining lateral rubber membrane boundary. The same techniques have been used to insert piezoceramic elements through the rubber membrane containing the sample in a Cubical Cell which permits the stresses on the boundaries of an initially cubical sample to be controlled at will so that stress paths in three dimensional principal stress space can be followed. Whereas samples prepared by gravitational deposition and mounted in the triaxial apparatus with their axis coincident with the direction of pluviation will always retain an axially symmetric symmetry of

* Department of Civil Engineering, University of Bristol, Queen's Building, University Walk, Bristol BS8 1TR, United Kingdom

Tab. I – Laboratory geophysical tests.
Tab. I – Test geofisici di laboratorio.

Test name	Description
BE-K1*	Isotropic compression ($K_o = 1$) to $p' = 300$kPa vertical direction in CC parallel to deposition direction ($z = v$)
BE-K1	Isotropic compression ($K_o = 1$) to $p' = 300$kPa horizontal direction in CC parallel to deposition direction ($x = v$)
BE-K2	Compression stress ratio $K_o = 2$ horizontal direction in CC parallel to deposition direction ($x = v$)
BE-K0.5	Compression stress ratio $K_o = 0.5$ horizontal direction in CC parallel to deposition direction ($x = v$)
BE-K1.5	Compression stress ratio $K_o = 1.5$ horizontal direction in CC parallel to deposition direction ($x = v$)
BE-H-con	Isotropic compression, shearing with constant horizontal stress horizontal direction in CC parallel to deposition direction ($x = v$)
BE-V-con	Isotropic compression, shearing with constant vertical stress horizontal direction in CC parallel to deposition direction ($x = v$)

their anisotropic stiffness properties, so that this stiffness can be described by a cross-anisotropic elastic model having 5 independent elastic properties, once the stress state imposed in the Cubical Cell departs from axial symmetry the symmetries of the anisotropy will also disappear, and additional elastic stiffnesses will be required to populate the stiffness matrix. The only simplification that is available is the continued alignment of the principal axes of anisotropy with the axes of the cube.

This paper briefly describes the technique that has been used to incorporate piezoceramic elements in the Cubical Cell and some of the results that have been obtained. The data presented have been obtained only from axially symmetric stress histories so that cross-anisotropy can be assumed. To fully determine all the components of the elastic stiffness matrix as the anisotropy evolves quite subtle testing is required, including the monitoring of waves sent on *inclined* paths between adjacent faces of the cube as well as paths *directly* between opposite faces. The challenges that are presented by the interpretation of such waves are discussed.

Apparatus and procedure

The stress-controlled Cubical Cell at Bristol [SADEK, 2006] was constructed based on designs supplied by the University of Colorado at Boulder [DEWOOLKAR *et al.*, 1997], a descendant of the cubical cell developed by KO and SCOTT [1967]. The apparatus (Fig. 1) consists of a stainless-steel frame surrounding a cubical void which houses the specimen contained within a latex rubber membrane. In each face of the frame a silicone rubber pressure cushion is provided to apply normal stress to the corresponding face of the sample; the air pressure in each cushion is measured by a pressure transducer located immediately behind the face. The cushions react against stainless-steel wall assemblies bolted and sealed to the frame. Displacements of each face of the sample are measured by a group of three Linear Variable Differential Transformers (LVDTs). Any desired stress path can be followed by means of a control program written with LabVIEW. Strain paths can in principle also be followed using control routines written with LabVIEW – but the configuration of the apparatus lends itself more naturally to stress histories.

The tests reported here have been performed on dry Hostun sand HS S28, an angular to sub-angular sand from south-east France. The particular sand grading used has $d_{50} = 0.34$mm and a uniformity coefficient $C_u = 1.5$, $e_{max} = 1.00$ and $e_{min} = 0.65$ [SADEK, 2006]. Samples for testing in the Cubical Cell were prepared by pluviation, following the multiple sieve procedure proposed by MIURA and TOKI [1982]. An extensive study of the effect of varying the parameters of this procedure ended with 6 sieves with mesh size 3.35mm and a final height of free fall of 450mm. This arrangement was found to give reproducibly uniform samples with relative density of 65%.

A laboratory geophysical technique based on the use of Bender/Extender elements (B/E elements) has been used in order to assess the elastic properties of the sand. The B/E element [LINGS and GREENING, 2001] is made from piezo-ceramic bimorph. Using appropriate electrical connections in relation to the polarisation of the constituent piezoceramic plates it is possible to excite the element in

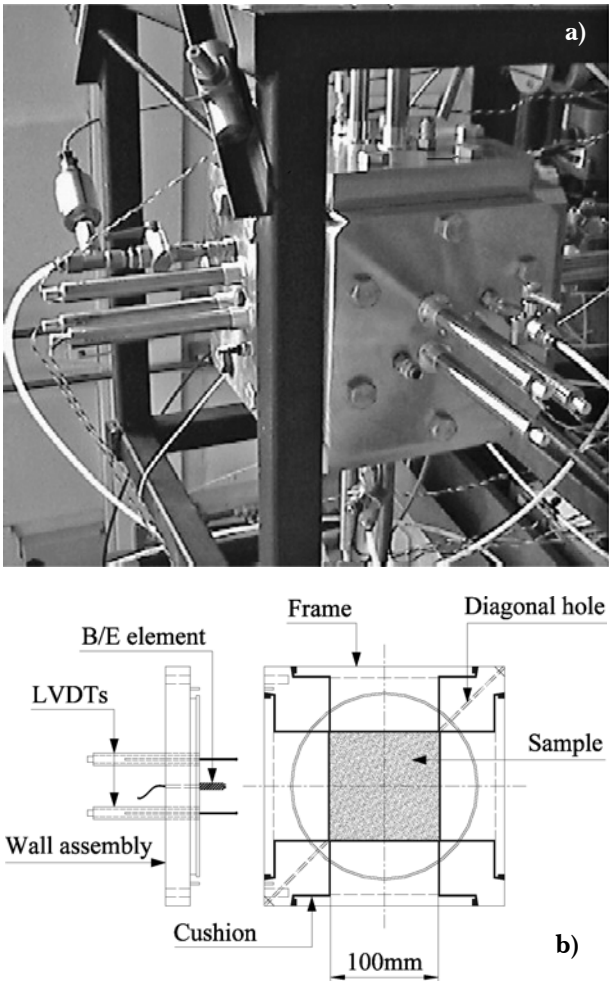

Fig. 1 – Cubical Cell: (a) assembled apparatus; (b) sections through reaction plates showing LVDTs and Bender/Extender elements.
Fig. 1 – Cella Cubica: (a) cella assemblata; (b) sezioni della cella con la posizione degli LVDT e degli elementi Bender/Extender.

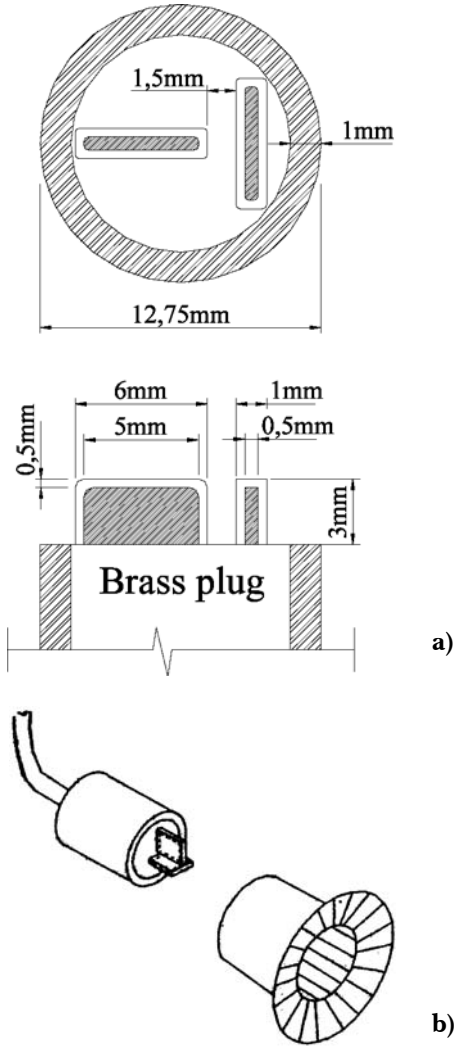

Fig. 2 – Bender/Extender elements: (a) sections through brass plug; and (b) grommet for mounting through flexible membrane.
Fig. 2 – Elementi Bender/Extender: (a) sezioni trasversali del tappo di ottone; e (b) foro di installazione attraverso la membrana flessibile.

such a way that it either bends (the classical use of bender elements) or extends and hence that the wave that is generated in the soil has dominant shear or compression characteristics respectively. Similar considerations apply to the receiver element which can be made sensitive primarily to either local shear displacement orthogonal to the element or to displacement along the axis of the element. A pair of B/E element installations on opposite sides of a soil sample can thus be used in principle to explore the shear wave velocities and the compression wave velocities in the soil. The B/E elements are glued into a brass plug in pairs to give a T-form arrangement (Fig 2): this enables shear waves to be generated and received with two different, orthogonal polarisations for virtually the same wave path.

In order to permit the insertion of the B/E elements in the sand samples a T-shaped cut, of the same size and shape as the B/E elements, was formed in the centre of four faces of the membrane and sealed with adhesive tape. The sample was pluviated into the membrane, and transferred to the Cubical Cell. Then for each of the four faces with B/E elements in turn, the adhesive tape was cut with a sharp blade and the pair of B/E elements in their brass plug housing surrounded with a sealing grommet were pushed about 3mm into the sample. The electrical connection to the B/E element was brought out through the centre of the stainless steel wall assembly and sealed with a specially designed threaded plug. Full details of these procedures can be found in SADEK [2006].

In the present programme of tests it was possible to install pairs of B/E elements in only five faces of the cubical sample: a technique has subsequently been developed to install them also in the bottom face of the sample. All six pairs are required in or-

der to deduce all nine parameters describing the orthorhombic elastic anisotropy which can develop under multiaxial stress states. However, by rotating the sample by 90° before it was inserted into the Cubical Cell, so that the depositional direction corresponded to one of the horizontal axes of the apparatus, sufficient information could be obtained using just four pairs of elements (Fig. 3), invoking material symmetries, to establish the five parameters which describe cross-anisotropic elastic anisotropy which suffices for axisymmetric stress states. The test configurations and stress conditions for these laboratory geophysical tests are listed in Table I. The term 'direct' will be used for waves that travel between opposite faces of the Cubical Cell (for example, between B/E elements 8 and 4 in Fig. 3) and the term 'inclined' will be used for waves that travel between adjacent faces of the Cubical Cell (for example, between B/E elements 8 and 2 in Fig. 3). Where the terms 'vertical' and 'horizontal' are used in the context of wave velocities or deduced stiffnesses these relate always to the vertical direction of deposition of the sample, whether or not this is actually in the vertical direction when the sample is tested in the Cubical Cell. The note $z = v$ or $x = v$ in Table 1 indicates with which axis the vertical pluviation direction coincides once the sample is mounted in the Cubical Cell.

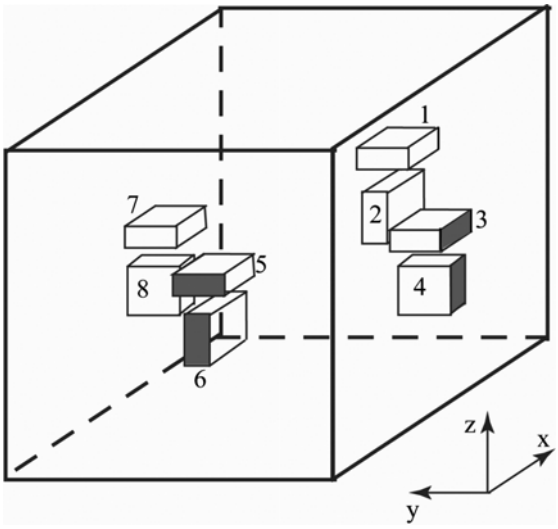

Fig. 3 – Pairs of Bender/Extender elements in boundaries of cubical cell: 1, 2 and 5, 6 face each other in x direction; 3, 4 and 7, 8 face each other in y direction; in test BE-K1* the z axis coincides with the direction of deposition; in other tests, the sample is rotated so that the vertical direction of deposition is horizontal and aligned with the x direction.
Fig. 3 – Coppie di elementi Bender/Extender sul contorno della cella cubica: 1, 2 e 5, 6 ai lati opposti in direzione x; 3, 4 e 7, 8 ai lati opposti in direzione y; nel test BE-K1 l'asse z coincide con la direzione di deposizione del campione; negli altri test, il provino viene ruotato in modo che la direzione di deposizione verticale diventi orizzontale ed allineata con la direzione x.*

Interpretation of dynamic tests

The velocity of transmission of a wave through an elastic medium is proportional to the square root of the corresponding stiffness. Thus can the stiffness properties be deduced from the wave velocities. Determination of the wave velocity requires the estimation of the time that it takes the wave to travel a known distance. We may be somewhat confident that the distance between transmitter and receiver elements can be represented by the distance between the centres of the tips of the elements [VIGGIANI and ATKINSON, 1995], whether the wave being studied is passing directly between opposite faces of the sample or inclined between B/E elements on adjacent faces. This was checked for sample BE-K1* by comparing estimated shear wave velocities for direct and inclined waves in the horizontal plane of isotropy (orthogonal to the direction of deposition) –

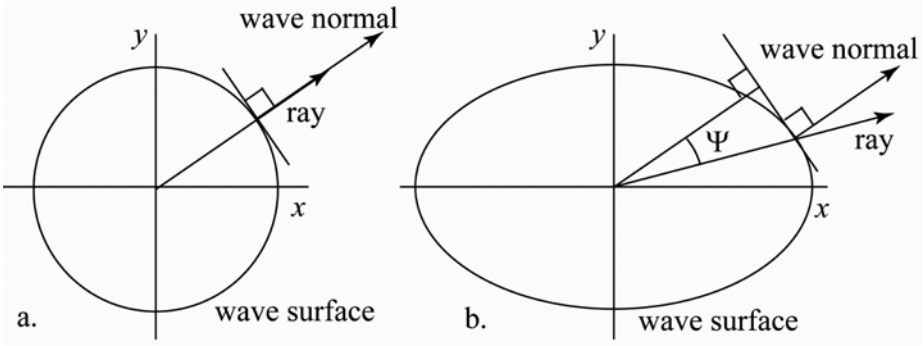

Fig. 4 – Directions of ray and wave normal on the wave surface from a point source in (a) isotropic full space (ray velocity = phase velocity); and (b) anisotropic full space (ray velocity = phase velocity/cos Ψ) [after STOKOE *et al.*, 1995].
Fig. 4 – Direzioni del raggio sismico e della normale al fronte d'onda per sorgente puntiforme in (a) mezzo isotropo; e (b) mezzo anisotropo [da STOKOE et al., 1995].

for example, between elements 7 and 3 and elements 7 and 1 respectively.

However, the objective deduction of the travel time – or more specifically the arrival time at the receiver element – remains challenging. At the time of the introduction of bender elements to laboratory soil testing, step waves (Heaviside functions) were frequently used to excite the transmitting element [DYVIK and MADSHUS, 1985; POROVIĆ, 1995]. However, such square waves have a very rich frequency content which exacerbates effects of wave dispersion; VIGGIANI and ATKINSON [1995] concluded from a Fourier signal cross-correlation analysis that the use of square input waves could lead to significant errors and suggested using a sine pulse as an input signal. Numerical techniques were then used to reduce the uncertainty in the arrival time to up to ±7%. JOVIČIĆ *et al.* [1996] proposed the use of a distorted sine wave, arguing that this shape would help to reduce near-field distortions [ARROYO *et al.*, 2003]. In fact, any pulsed rather than continuous input signal will contain energy at frequencies other than the dominant frequency.

On the basis of experience at Bristol with different input signal waveforms [PENNINGTON *et al.*, 1997; SADEK, 2006], a single symmetrical sinusoidal pulse (Fig. 5) was used with amplitude 20V peak to peak and frequency chosen to ensure that there are sufficient wavelengths between transmitter and receiver. Standardising on a single pulse shape removes a source of variability so that at least relative effects can be confidently observed.

Wave paths in the cubical cell

The tests reported here, even though performed in the true triaxial Cubical Cell, have maintained the axial symmetry of the original vertical direction of deposition. The stiffness properties are therefore expected to be consistent with a cross-anisotropic elastic model defined by a stiffness matrix with 5 independent elastic parameters. The stiffness matrix is written here with the z direction coincident with the vertical direction of deposition as in test BE-K1*.

$$\begin{bmatrix} \Delta\sigma'_{xx} \\ \Delta\sigma'_{yy} \\ \Delta\sigma'_{zz} \\ \Delta\tau_{yx} \\ \Delta\tau_{zx} \\ \Delta\tau_{xy} \end{bmatrix} = \begin{bmatrix} C_{11} & C_{12} & C_{13} & 0 & 0 & 0 \\ C_{12} & C_{11} & C_{13} & 0 & 0 & 0 \\ C_{13} & C_{13} & C_{33} & 0 & 0 & 0 \\ 0 & 0 & 0 & C_{44} & 0 & 0 \\ 0 & 0 & 0 & 0 & C_{44} & 0 \\ 0 & 0 & 0 & 0 & 0 & C_{66} \end{bmatrix} \begin{bmatrix} \Delta\varepsilon_{xx} \\ \Delta\varepsilon_{yy} \\ \Delta\varepsilon_{zz} \\ \Delta\varepsilon_{yz} \\ \Delta\varepsilon_{zx} \\ \Delta\varepsilon_{xy} \end{bmatrix} \quad (1)$$

where

$C_{11} = M'_h$ = horizontal constrained modulus

$C_{33} = M'_v$ = vertical constrained modulus

$C_{44} = G'_{vh}$ = shear modulus in a plane including the axis of symmetry

$C_{66} = G'_{hh}$ = shear modulus in the plane of isotropy

$C_{12} = M'_h - 2\,G'_{hh}$ (and thus not an independent stiffness quantity)

C_{13} = ratio of increments of horizontal stress and vertical strain under one-dimensional compression – a fifth independent elastic quantity

Study of (1) shows that C_{11} and C_{33} can be obtained from compression wave transmission in horizontal and vertical directions while C_{44} and C_{66} can be obtained from shear waves propagating in a horizontal direction with vertical and horizontal polarisation respectively. That leaves C_{13} which has to be estimated in a more complex manner using inclined seismic body waves.

For the simple case of an isotropic and homogeneous medium the shape of the propagating body wave through any principal plane is circular. Body waves propagating through anisotropic soils have a somewhat elliptical propagation surface, with the elongation of the 'ellipse' increasing as the degree of anisotropy increases [STOKOE *et al.*, 1995]. For an anisotropic soil, the ray velocity V_{ray} measured directly from the wave travel time and distance, does not coincide with the phase velocity V_{phase} that is required for the assessment of the elastic constants (Fig. 4). The two velocities are linked:

$$V_{phase} = V_{ray}\ \cos\Psi \quad (2)$$

where Ψ is the angle between the normal to the wave surface and the ray direction (Fig. 4). STOKOE *et al.* [1991] and LEE [1993] determined the value of Ψ experimentally for dry silica sands, and found it to be 10°, so that only a minor correction of the measured ray velocity is required to deduce the phase velocity: no correction has been applied in the present study (following BELLOTTI *et al.*, 1996; and FIORAVANTE, 2000).

Considering *P*- and *S*-waves propagating in the vertical plane and arriving from a direction making an angle $\grave{e}$ with the vertical z-axis, the following expression for body wave velocities (attributed by WHITE [1983] to STONELEY [1949] and also quoted by BELLOTTI *et al.* [1996] and FIORAVANTE, [2000]) can be deduced:

$$V_{P\theta} = \sqrt{\frac{(M'_h \sin^2\theta + M'_v \cos^2\theta + G'_{vh} + \Delta)}{2\rho}} \quad (3a)$$

$$V_{S\theta,v} = \sqrt{\frac{(M'_h \sin^2\theta + M'_v \cos^2\theta + G'_{vh} - \Delta)}{2\rho}} \quad (3b)$$

$$V_{S\theta,h} = \sqrt{\frac{(G'_{hh} \sin^2\theta + G'_{vh} \cos^2\theta)}{\rho}} \quad (3c)$$

where

$$\Delta=\sqrt{\begin{matrix}[(M'_h-G'_{vh})\sin^2\theta-(M'_v-G'_{vh})\cos^2\theta]^2\\+4(C_{13}+G'_{vh})^2\sin^2\theta\cos^2\theta\end{matrix}} \qquad (4)$$

$V_{P\theta}$ is the velocity of the *P*-wave travelling along an axis rotated by the angle θ with respect to the vertical axis, $V_{S\,\theta,v}$ is the propagating velocity of a shear wave travelling along an axis rotated by the angle θ with respect to the axis of vertical deposition with particle motion in a vertical plane, $V_{S\,\theta,h}$ is the velocity of the *S*-wave propagating along an axis rotated by the angle θ with respect to the axis of vertical deposition with horizontal particle motion and ρ is the bulk density of the medium. In general, the value of C_{13} can be computed either from (3a) or from (3b) in conjunction with (4). There is thus the possibility of two independently determined values of C_{13}.

In the present tests, four pairs of B/E elements were installed in the four vertical sides of the cubical sample, where in general the vertical deposition direction of the sample had been rotated to coincide with one of the horizontal directions (Tab. I and Fig. 3). Direct waves were sent between elements in

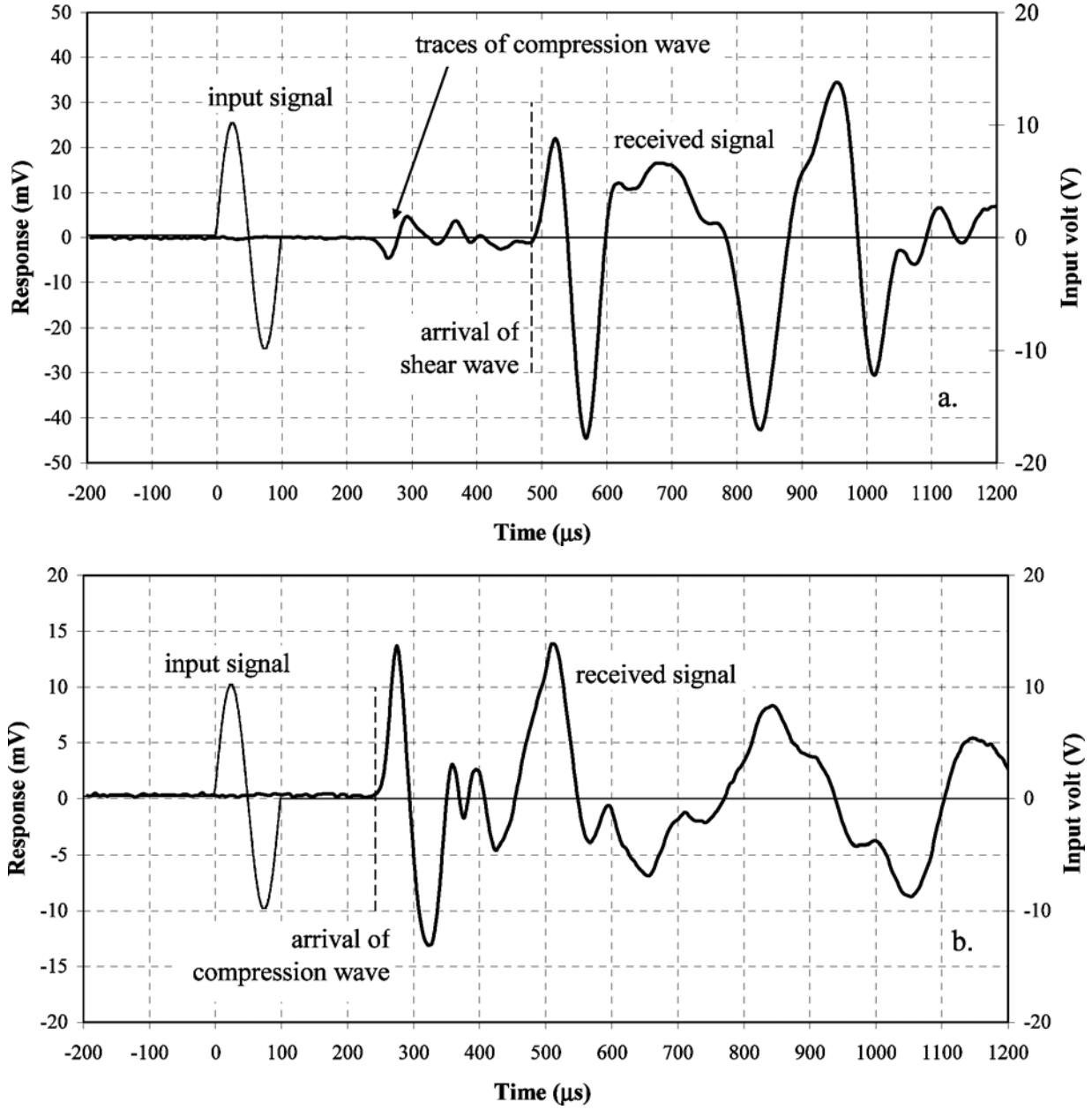

Fig. 5 – Test BE-K1*, p' = 50kPa: (a) absolute response of S_{xz} (from element 5 to element 1); (b) absolute response of P_{x1} (from element 2 to element 6).

Fig. 5 – Prova BE-K1, p' = 50kPa: esempi di segnali corrispondenti ad (a) onda S_{xz} (dall' elemento 5 all'elemento 1); (b) onda P_{x1} (da 2 a 6).*

opposite faces of the cube, and inclined waves were sent along directions at 45° to the axes of the cube. The following elastic constants could then be determined. (The final numerical subscript indicates the originating B/E element.)

M'_v calculated from compression waves from elements 1 or 2 to elements 5 or 6: $V_{P\,\mathrm{v1}}$, $V_{P\,\mathrm{v2}}$

M'_h calculated from compression waves from elements 3 or 4 to elements 7 or 8: $V_{P\,\mathrm{h3}}$, $V_{P\,\mathrm{h4}}$

G'_{vh} calculated from shear waves from elements 5 or 6 to elements 1 or 2: $V_{S\,\mathrm{vh5}}$, $V_{S\,\mathrm{vh6}}$

G'_{hv} calculated from shear waves from element 8 to element 4: $V_{S\,\mathrm{hv8}}$

G'_{hh} calculated from shear waves from element 7 to element 3: $V_{S\,\mathrm{hh7}}$

M'_{45} calculated from 45° compression waves from elements 1, 2, 3, 4 to elements 7, 8, 5, 6 respectively: $V_{P\,45,1}$, $V_{P\,45,2}$, $V_{P\,45,3}$, $V_{P\,45,4}$

$G'_{45,v}$ calculated from 45° shear waves from elements 8 or 6 to elements 2 or 4: $V_{S\,45,\mathrm{v8}}$, $V_{S\,45,\mathrm{v6}}$

$G'_{45,h}$ calculated from 45° shear waves from elements 7 or 5 to elements 1 or 3: $V_{S\,45,\mathrm{h7}}$, $V_{S\,45,\mathrm{h5}}$

Presentation of results

A pair of wave responses for *S*-waves and *P*-waves propagating in opposite directions through the same sample (from element 5 to element 1 and from element 1 to element 5 respectively) are shown in Figs. 5a, b. (It is a consequence of the wiring required to produce the bending or extending modes of deformation that the most effective mode of operation interchanges transmitter and receiver for compression and shear waves.) It is evident that the point of first deflection in the two waveforms occurs at more or less the same time: it seems reasonable to associate this first arrival with the (unintended) compression wave generated by the bender elements (see BRIGNOLI and GOTTI, 1992).

Assuming that the soil is indeed cross-anisotropic there is considerable potential redundancy in the measurements. For example, it is confirmed that the arrival time for *P*-waves propagating from Extender elements oriented in the *y* direction (for example, from 3 to 7 in Fig. 3) is identical to that for waves transmitted in the same direction from orthogonal elements (for example, from 4 to 8): the *P*-wave velocity is independent of the Extender element orientation inside the sample. This would have been anticipated from the expression proposed by ROESLER [1979] (discussed below) which links wave velocities with the product of the principal stresses in the direction of propagation and direction of polarisation. 'Polarisation' does not really have a meaning for *P*-waves but it can be thought of as the direction of particle motion which for these waves coincides with the direction of propagation. Roesler's 'law' thus implies that a compression wave velocity (along a coincident principal axis of stress and material anisotropy, to be specific) is influenced only by the principal stress in the direction of propagation. Further observations of shear wave and compression wave propagation confirm the hypothesis of cross-anisotropic elasticity with an axis of symmetry coinciding with the direction of pluviation.

The dependence on mean stress of various measured direct and inclined wave velocities in a horizontal plane of isotropy is shown in Figs. 6a, b. In general, multiple measurements of the same wave velocity between different pairs of B/E elements show close agreement, as demonstrated by the closeness of the three groupings in Figs. 6a (P_{h}, S_{hh}, S_{hv}) and 6b ($P_{45,\mathrm{h}}$, $S_{45,\mathrm{hh}}$, $S_{45,\mathrm{hv}}$). Velocities from direct and inclined waves are compared in Fig 6c: the line with slope 1 links results with the same velocity. Velocities from inclined and direct body wave measurements agree well for *P*-waves and *S*-waves with vertical polarisation. However, inclined shear waves with horizontal polarisation show higher velocities than their direct counterparts with a ratio of velocities of around 1.25. The most obvious explanation for this result is that the mode of horizontally polarised bender deformation of B/E element 8 (for example) tends to generate a more significant compression wave component in the direction of the receiving element 2 by comparison with the vertically polarised wave being sent from B/E element 7 to be received by element 1. In no case is the transmitter element producing a pure shear deformation of the sand and there is evidently a likelihood that the element is squeezing and compressing the soil – the extent to which this compression energy is able to swamp the shear wave arrival depends on the attenuation that occurs in the sand.

Where measurements of shear wave velocity are made both for horizontal propagation with vertical polarisation and for vertical propagation with horizontal polarisation it has been observed by some researchers that there is a small difference between the two values even though they should be identical for an elastic material. (Though there may be effects linked to the way in which shear waves are transmitted in addition to effects of the non-point-like nature of the shear wave source which may tend to lead to an apparent asymmetry of the *deduced* stiffness matrix in anisotropic elastic soil [ARROYO, 2001; ARROYO and MUIR WOOD, 2004]). Results obtained from the present Cubical Cell tests – with the sample rotated to make the vertical direction of deposition correspond with the *x* direction of the apparatus, so that shear wave velocities V_{Syx} (from element 8 to element 4) and V_{Sxy} (from element 6 to element 2) are being compared – suggest that the former wave travels consistently around (on average) 3% faster

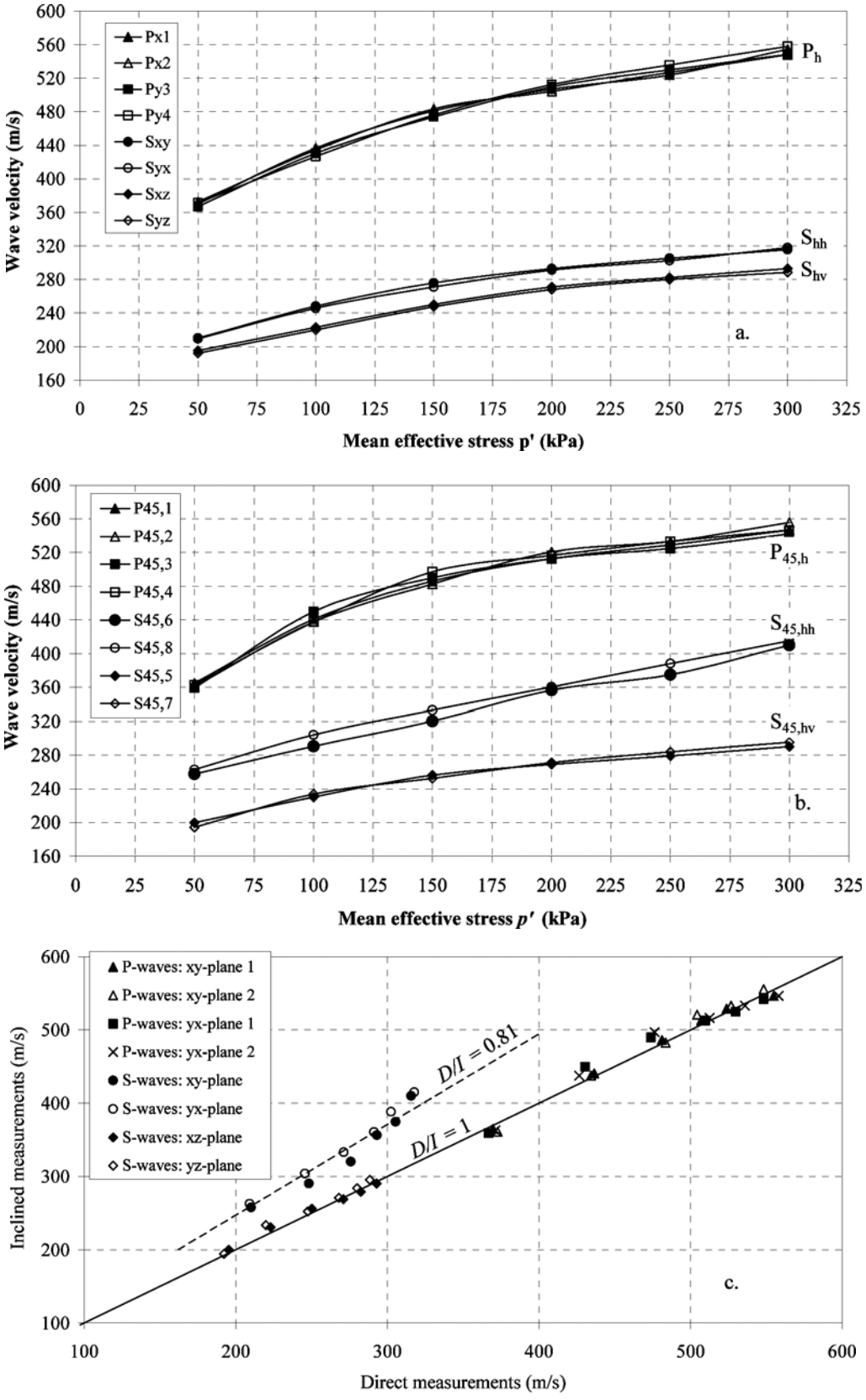

Fig. 6 – (a) Velocity of direct body waves propagated in test BE-K1*; (b) velocity of inclined body waves propagated in test BE-K1*; (c) relationship between direct and inclined velocity measurements for different wave types (test BE-K1*).
Fig. 6 – (a) Velocità delle onde di volume dirette nella prova BE-K1; (b) velocità delle onde di volume inclinate nella prova BE-K1*; (c) relazione tra misure di velocità delle onde dirette ed inclinate per diversi tipi di onde (prova BE-K1*).*

than the latter: $V_{Shv} > V_{Svh}$. KUWANO *et al.* [2000] and PENNINGTON *et al.* [2001] have observed similar disparities between the deduced values of G'_{hv} and G'_{vh} and have attributed this to the different boundary conditions in the conventional triaxial cell, the sample geometry or to differences in the dimensions of the bender elements: but none of these arguments can be applied to the dynamic measurements in the Cubical Cell. It might be concluded that an elastic interpretation of sand response is not valid even at the small strain level of the bender perturbation – but the discrepancy is small. For the purposes of estimation of elastic properties here the shear modulus G'_{vh} will be taken as the average of the G'_{hv} and G'_{vh} measurements.

Under isotropic effective stresses, waves propagating in the horizontal direction of the sample travel faster than those transmitted in the vertical direction. This outcome reflects the degree of inherent anisotropy of Hostun sand samples due to pluviation. This feature is more pronounced with respect to *P*-waves than *S*-waves. A mean value of $H/V = 1.17$ is obtained from *P*-waves (Fig. 7), whereas for *S*-waves the average ratio of *H/V* was found to be 1.10. These values are comparable with values quoted by BELLOTTI *et al.* [1996] and FIORAVANTE [2000] testing Ticino sand. BELLOTTI *et al.*, for example, give *H/V* values for *P*-waves of 1.08 and 1.13 in medium dense and very dense samples respectively and for *S*-waves of around 1.1 and 1.07 in medium dense and very dense samples. The implication for these sands is clearly that the horizontal direct stiffness is greater than the vertical direct stiffness under the 'constant fabric' test conditions of the Bender/Extender tests. Discrete element modelling of the process of generation and propagation of waves through (idealised) particulate materials might throw light on the extent to which such wave propagation can be reliably interpreted as 'elastic' and on the nature of the fabric changes that would accompany different stress or strain histories.

Modelling of stiffness variation with stress

ROESLER [1979] proposed an expression which describes the way in which stiffnesses deduced from wave propagation should be influenced by the principal stresses in and orthogonal to the directions of propagation. The general form for a shear modulus deduced from propagation in direction *a* and with polarisation direction *b* is then:

$$G_{0_{(ab)}} = C_{G_{(ab)}} f(e) \left[\frac{\sigma'_a}{P_a}\right]^{N_a} \left[\frac{\sigma'_b}{P_a}\right]^{N_b} \left[\frac{\sigma'_c}{P_a}\right]^{N_c} \qquad (5)$$

where C_{Gab} is a reference value for the particular modulus under consideration and $f(e)$ is a function of void ratio. The three principal stresses are normalised by a reference pressure (atmospheric pressure is typically used though it would be more appropriate to use some material property such as tensile strength of the sand mineral) and raised to exponents N_a, N_b, N_c which are material constants. A modest extrapolation and generalisation of (5) pro-

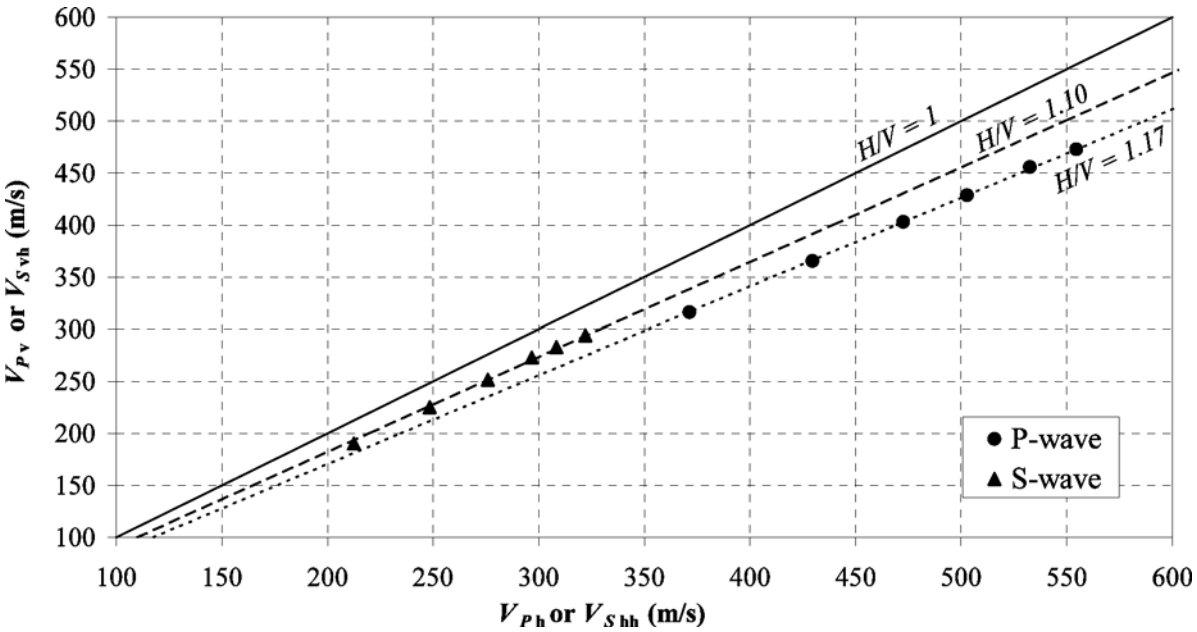

Fig. 7 – Evaluation of inherent anisotropy in Hostun sand sample (test BE-K1): ratios of compression wave velocities and shear wave velocities.

Fig. 7 – Valutazione dell'anisotropia intrinseca in un campione di sabbia di Hostun (prova BE-K1): rapporti tra la velocità delle onde di compressione e di taglio.

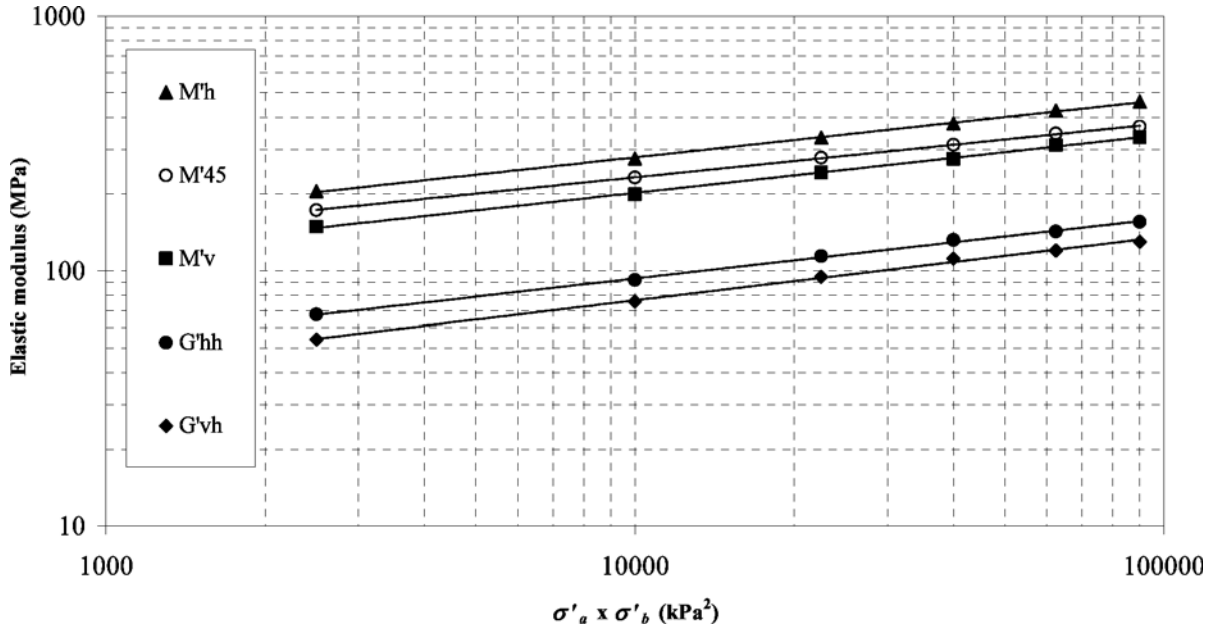

Fig. 8 – Cross-anisotropic elastic moduli obtained from test BE-K1.
Fig. 8 – Moduli elastici trasversalmente anisotropi ottenuti dalla prova BE-K1.

duces an essentially similar expression for constrained moduli as well as shear moduli – the propagation and polarisation directions then coincide. It is typically found that $N_c \approx 0$ and that the stress orthogonal to the plane containing the propagating wave has negligible influence on the wave velocity. On the other hand, inclined propagating waves do not fit so neatly into the expected pattern: the directions of propagation and polarisation are no longer aligned with axes of principal stress.

Figure 8 shows the variation of several stiffness parameters as a function of the corresponding respective products of effective stresses $\sigma'_a \sigma'_b$ for the test, BE-K1, with isotropic compression. Each data point is the average of the available velocity measurements converted into moduli. From this plotting it is not possible to separate values of N_a and N_b and they have to be assumed equal. A summary of values of the stress exponent from a number of tests is given in Table II. The data confirm that the sum of values of N_a and N_b is around 0.5 – so that the stiffness is approximately proportional to square root of stress.

For all the tests it is assumed that the volumetric strains are sufficiently small that $f(e)$ can be treated as a constant which can be incorporated into C_G. From the isotropic and three anisotropic compression tests following constant K paths the values of $(N_a + N_b)$ for the different stiffness parameters can be deduced together with the material constants C_G or C_M. The values of $(N_a + N_b)$ vary from 0.425 (slope of M'_{45} from test BE-K1) to 0.561 (slope of G'_{hh} from test BE-K0.5) and are within the range of values quoted in the literature. However, it appears that these exponents tend to decrease as the compression stress ratio increases. The stress exponents are also slightly higher for G moduli than for M moduli (a similar result was presented by SOMFAI *et al.* [2005] based on numerical simulations of acoustic wave propagation in confined granular deposits): there is not yet an explanation for this difference. The high values of the correlation coefficient R in Table II provide confidence in the parameters with which the data have been fitted.

The expression proposed by Roesler assumes for simplicity (and based on experimental observation) that the wave velocities are not influenced by the principal stress orthogonal to the plane containing the directions of propagation and polarisation. The influence should be especially visible for compression waves: KUWANO and JARDINE [2002], LEWIS [1990] and STOKOE *et al.* [1991] concluded that M'_h is a function of σ'_h only, and M'_v depends solely on σ'_v. Figure 9 shows the constrained moduli obtained from all constant stress ratio paths for common values of the horizontal stress. The dominant increase in M'_v values as σ'_v increases is expected but there seems to be a negative trend for M'_h values. A similar pattern of response is found for M'_v values when collected from stress states for which the vertical stress has the same value and again modestly negative slopes are seen. Comparable relationships were presented by BELLOTTI *et al.* [1996] showing noticeable negative cross-dependence of M'_v on σ'_h. The present data have been collected from separate tests which happen to pass through related stress states rather than from individual tests on single specimens in which certain stress components are held

Tab. II – Material constants obtained from constant stress ratio paths.
Tab. II – Costanti dei materiali ottenute da percorsi a rapporto di carico costante.

Compression stress ratio *K*	**Modulus**	***N_a* + *N_b***	**Correlation coefficient *R***	***C_G f*(*e*) or *C_M f*(*e*) MPa**
0.5	M'_h	0.555	0.999	18.2
	M'_{45}	0.524	0.999	19.3
	M'_v	0.515	0.996	19.5
	G'_{hh}	0.561	0.999	6.5
	G'_{vh}	0.557	0.999	6.2
1	M'_h	0.453	0.999	34.6
	M'_{45}	0.425	0.999	32.8
	M'_v	0.457	0.999	24.6
	G'_{hh}	0.472	0.999	10.6
	G'_{vh}	0.499	0.998	7.7
1.5	M'_h	0.498	0.999	27.0
	M'_{45}	0.473	0.998	27.1
	M'_v	0.471	0.999	23.2
	G'_{hh}	0.539	0.999	7.2
	G'_{vh}	0.532	0.999	6.5
2	M'_h	0.482	0.999	33.4
	M'_{45}	0.472	0.999	29.5
	M'_v	0.456	0.997	24.6
	G'_{hh}	0.449	0.999	14.40
	G'_{vh}	0.488	0.998	8.46

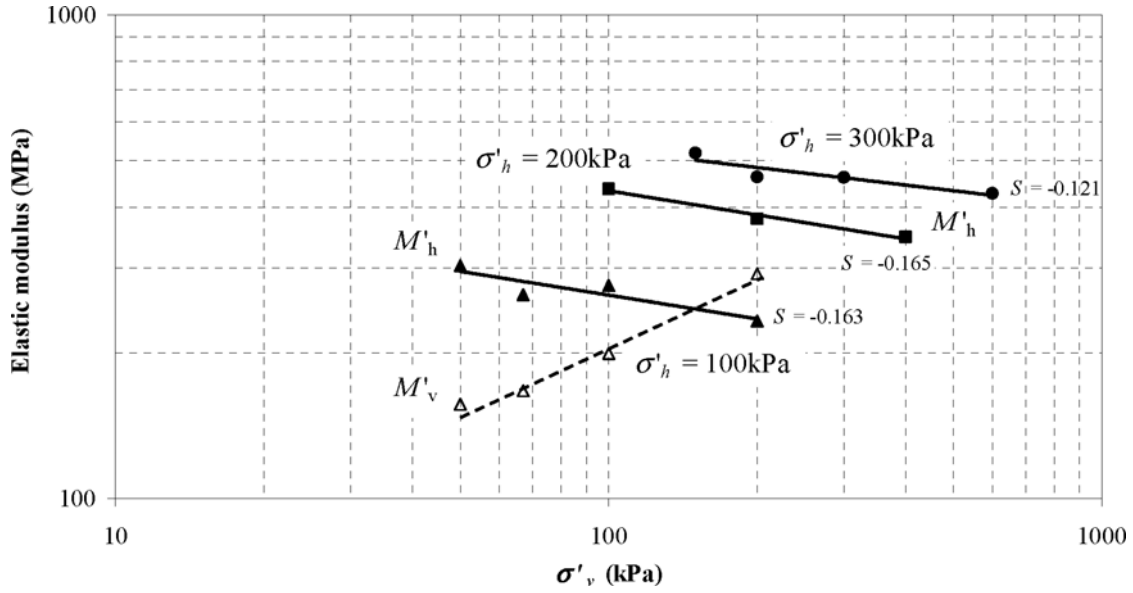

Fig. 9 – Influence of σ'_v on constrained moduli (σ'_h constant): open symbols: M'_v; solid symbols: M'_h.
Fig. 9 – Influenza di σ'_v sui moduli confinati (a σ'_h costante): simboli vuoti: M'_v*; simboli pieni:* M'_h.

constant. The present results thus test a rather broad picture of the model of evolution of elastic properties.

Elastic properties of Hostun sand

The cross-anisotropic elastic stiffness of Hostun sand at small strain levels is described by the stiffness matrix [C] of Equation (1), with five independent elastic constants. The values of C_{11}, C_{33}, C_{44} and C_{66} in (1) correspond to M'_h, M'_v, G'_{vh} and G'_{hh}, which are determined without difficulty from direct body wave measurements. The value of C_{13} requires velocities for inclined wave transmission: various expressions can be found from manipulation of Equations (3a) (3b) and (4), for the experimental case of $\theta = 45°$. The inclined constrained modulus is defined as:

$$C_{13}=\frac{(M'_h+M'_v)+2G'_{vh}+\sqrt{(M'_h-M'_v)^2+4(C_{13}+G'_{vh})^2}}{4} \quad (6)$$

Then by inverting the expression C_{13} is given by:

$$M'_{45}=\sqrt{M'_hM'_v+(G'_{vh}-2M'_{45})(M'_h+M'_v+G'_{vh}-2M'_{45})}-G'_{vh} \quad (7)$$

Alternative expressions involving $G_{45,v}$ can be obtained for C_{13} but because of problems with $V_{S\,45,v}$ measurements the hoped for redundancy in determination of C_{13} has not been achieved.

In assessing the resulting stiffness values, an initial assumption has been made that the variation in void ratio within and between tests is negligible in its effect on the small strain stiffness. This allows us then to concentrate on the first order effects of stress history and stress state on the deduced stiffnesses.

The stiffness C_{13} describes coupling between stress and strain changes in a vertical plane containing the axis of depositional symmetry of the sample and its anisotropy. In trying to understand the way in which C_{13} varies with stress state it might appear reasonable to seek to correlate it with the principal stresses in this plane, which are the vertical and horizontal effective stresses in the sample. Figure 10 explores this correlation but reveals no particularly clear pattern of variation of C_{13} with stress level expressed in this way. There may be a general tendency for C_{13} to rise with increasing stresses for most compression stress ratios K, but at the higher stresses there appears to be a slight fall.

At constant compression stress ratio K the ratios M'_h/M'_v and G'_{hh}/G'_{vh} are somewhat constant with increasing stress level, but the ratios are influenced by the value of K (Fig. 11). Each point in this figure is an average value taken from the corresponding constant stress ratio compression test. The ratio G'_{hh}/G'_{vh} increases from 0.9 to 1.61 while K changes from 0.5 to 2. The variation in M'_h/M'_v ratios is much more pronounced increasing from 0.79 up to 2.07 for the same range of K. At a compression stress ratio of around 0.7 we might infer that the response of the sand would in fact be isotropic and this same conclusion might be drawn from the wave propagation surfaces presented in the next section. In general these power law relationships are as expected from Roesler's 'Law': we could predict that M'_h/M'_v

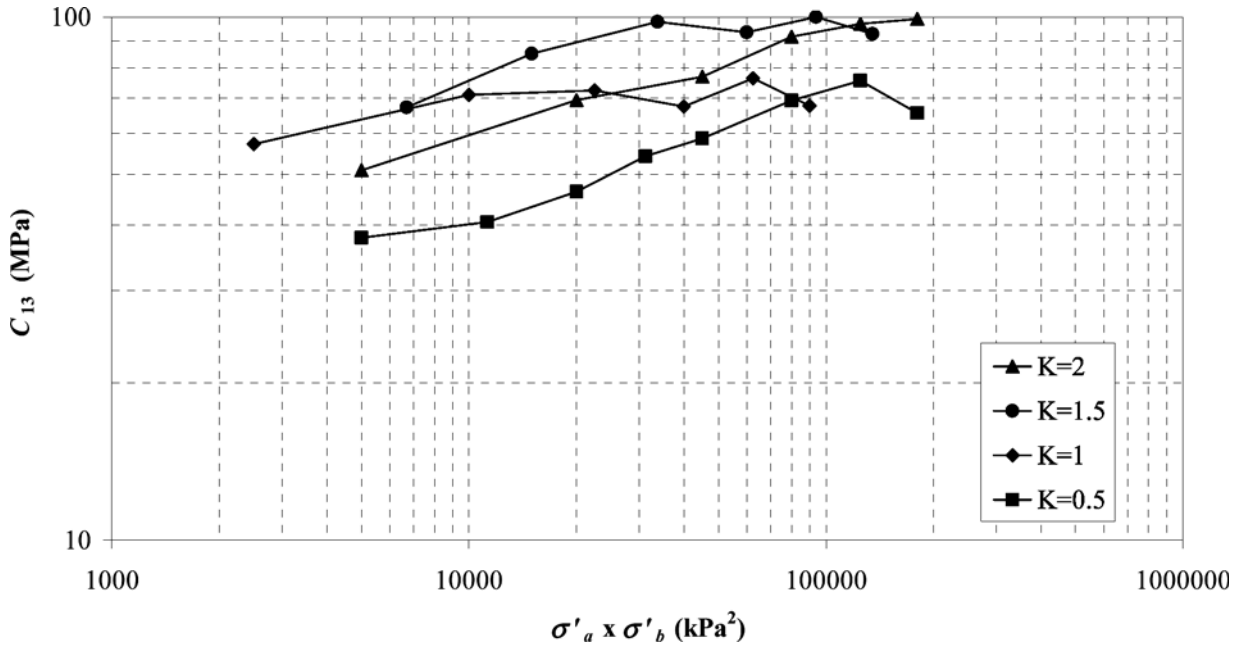

Fig. 10 – C_{13} plotted against σ'_a x σ'_b from constant stress ratio paths.
Fig. 10 – C_{13} in funzione di σ'_a x σ'_b per percorsi a rapporto tensionale costante.

would have the strongest dependence on K while G'_{hh}/M'_h could be predicted to remain constant.

Wave propagation surfaces

The compression stress ratio also has an effect on the shape of the surface of wave propagation. Considering the elastic constants determined at a certain stress level, it is possible to plot the surfaces for the three wave types ($V_{P\theta}$, $V_{S\theta,v}$ and $V_{S\theta,h}$) generated in a vertical section of the sample using Equations (3) and (4) as a function of θ. Figure 12 collects the several surfaces for the different values of K. The surfaces have been determined from the experimental observations for vertical and horizontal body waves and inclined compression waves so these values automatically sit on their appropriate curves. The remaining observations made for inclined wave paths can be used to confirm the implied shape. The shear waves with horizontal polarisation ($V_{S45,h}$: for example, between elements 7 and 1 in Fig. 3) (recalling that 'horizontal' is defined relative to the vertical direction of deposition which is aligned with the x axis in Fig. 3) reveal wave velocities which plot close to the shear wave propagation surface (Fig. 12). However, the shear waves with vertical polarisation ($V_{S45,v}$: for example, between elements 8 and 2 in Fig. 3) show anomalously high velocities which plot close to the *compression* wave propagation surfaces (Fig. 12), thus confirming the conclusion drawn earlier that the received wave is dominated by compression wave energy.

Figure 12 shows the progressive change in shape of the propagation surfaces as the compression stress ratio K increases from 0.5 to 2. The sections become progressively flatter (the ratio of horizontal velocities to vertical velocities becomes greater) as K increases: the body wave velocities in Hostun sand specimens are influenced to a larger extent by the stress-induced anisotropy than by inherent anisotropy. From these sections also (as from the stiffness ratios in Fig. 11) one might speculate that for a compression stress ratio between 0.5 and 1 (and closer to 0.5) the propagation surface would be circular and the stiffness isotropic.

Conclusion

Dynamic body wave measurements have been performed on dry Hostun sand samples in a multiaxial Cubical Cell using pairs of Bender/Extender (B/E) elements capable of transmitting and receiving *S*- and *P*-waves through the soil deposit, from which the elastic shear and constrained moduli could, in principle, be deduced. Pairs of B/E elements were installed through the flexible boundaries of the cubical cell specimens and measurements of wave velocity were made for direct wave paths between opposite faces of the sample and also for inclined paths between B/E elements on adjacent faces in order to deduce the full set of anisotropic elastic parameters.

A time domain procedure was used for the interpretation of the received signals in order to estimate arrival times and hence the corresponding wave velocities. Arrival times are not always easily and objectively discerned and, in particular, faster com-

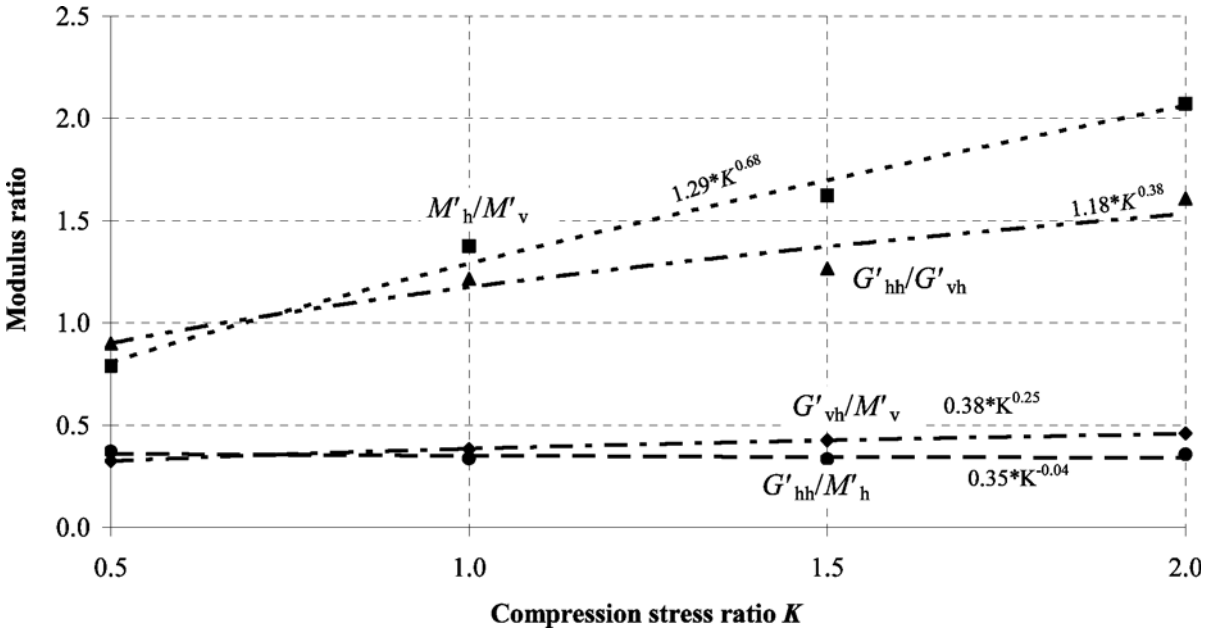

Fig. 11 – Influence of compression stress ratio K on ratios of moduli.
Fig. 11 – Influenza del rapporto tensionale K sui rapporti dei moduli.

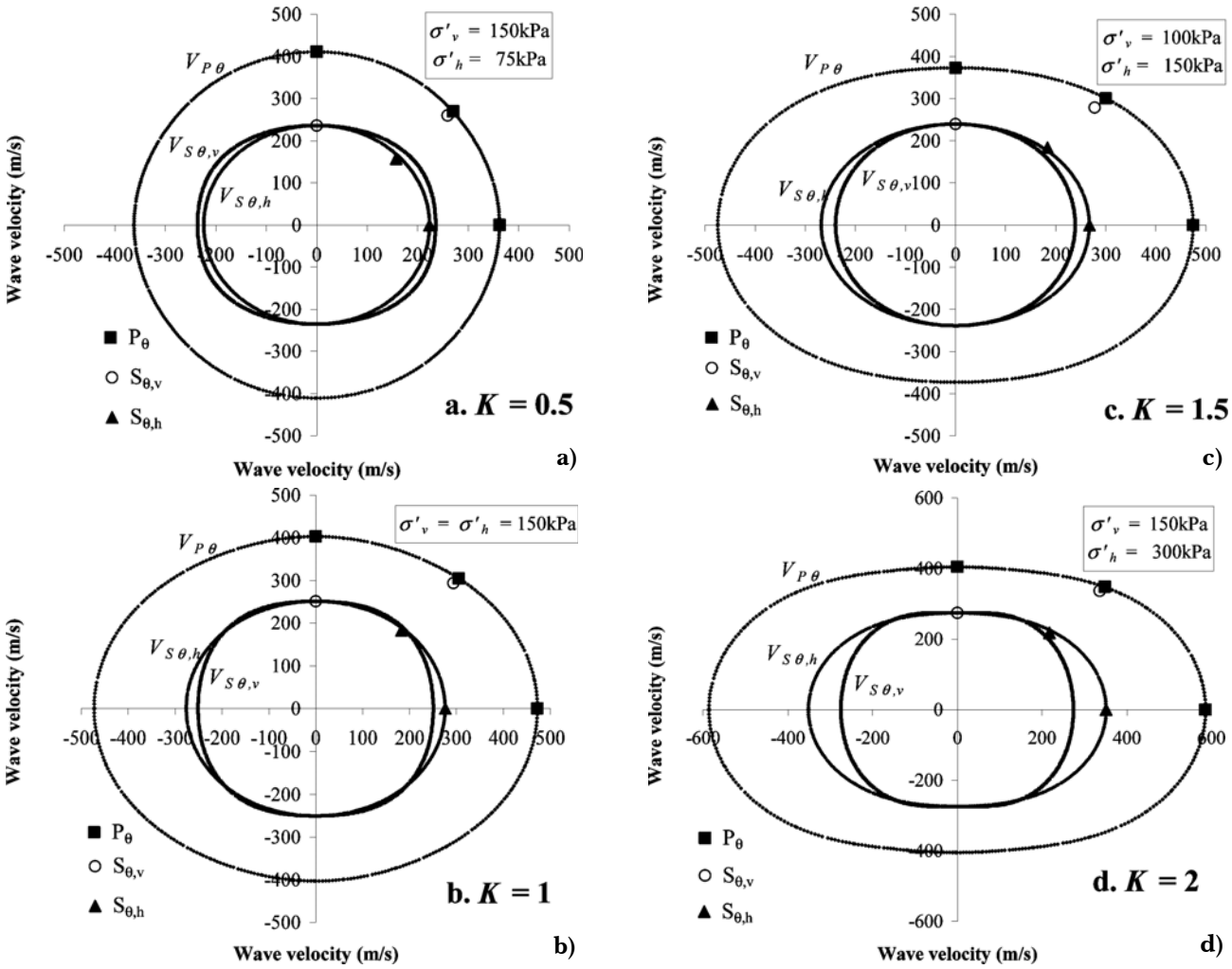

Fig. 12 – Wave propagation surfaces from tests with compression stress ratio: (a) 0.5; (b) 1; (c) 1.5; (d) 2.
Fig. 12 – Superfici di propagazione delle onde dalle prove con rapporto tensionale pari a: (a) 0.5; (b) 1; (c) 1.5; (d) 2.

pression wave energy tends to pollute the nominally slower shear wave motion as a result of boundary reflections or other effects. It was found difficult to detect shear wave arrival times from inclined paths with vertical polarisation (inclined waves with horizontal polarisation behaved more nearly as intended).

For the tests reported here, B/E elements were installed in four of the six faces of the cubical sample. It was possible thus to populate the elastic stiffness matrix for axially symmetric conditions and the stress paths followed maintained this symmetry about the vertical axis of pluviation – which was arranged to be a horizontal axis for the installed sample – leaving 5 elastic parameters to be determined. In principle this implies some redundancy in the measurements but this was reduced by the undesired compression/shear wave interaction.

Under isotropic stress conditions the ratios of various moduli demonstrate the degree of inherent anisotropy of freshly pluviated Hostun sand samples. Under anisotropic compression the degree of anisotropy depends on the imposed stress ratio: the ratios M'_h/M'_v and G'_{hh}/G'_{vh} increase with increase of the compression stress ratio, K. In contrast the ratios G'_{hh}/M'_h and G'_{vh}/M'_v remain constant.

There is some evidence from these as from tests of others that the shear wave velocities with horizontal propagation and vertical polarisation and with vertical propagation and horizontal polarisation are not quite the same. This observation has not yet been satisfactorily explained but may be linked to the nature of wave transmission in a particulate material [ARROYO and MUIR WOOD, 2004].

The combination of the multiaxial Cubical Cell and Bender/Extender elements forms a powerful and extremely sophisticated piece of soil testing equipment and enables the performance in an element test (with modest dimensions) of the suite of measurements that BELLOTTI *et al.* [1996] performed in a large calibration chamber. The observations made have demonstrated the utility of these piezo-

electric devices which combine the bender and extender deformation modes so that an extensive range of compression and shear wave velocities can be obtained from a common configuration. The interpretation of inclined wave propagation, which is essential for the complete population of these anisotropic stiffness matrices, is challenging because of the difficulty in propagating pure shear waves. There is a richness in the recorded information of received signals which remains to be fully exploited for deconvolution purposes. Extracting only the arrival time from the received trace ignores other messages that the elaborate attenuated waveforms are trying to persuade us to appreciate.

Acknowledgements

This work was performed with the support of a research grant from the UK Engineering and Physical Sciences Research Council (GR/R05260/01) *Multiaxial stiffness of sand*. Technical assistance from the Department of Civil Engineering and the Faculty of Engineering at Bristol University is gratefully acknowledged.

References

ARROYO M. (2001) – *Pulse tests in soil samples*. PhD Thesis, University of Bristol.

ARROYO M., MUIR WOOD D. (2004) – *Discussion: On the applicability of cross-anisotropic elasticity to granular materials at very small strains*. Géotechnique, 54, n. 1, pp. 75-76.

ARROYO M., MUIR WOOD D., GREENING P. (2003) – *Source near-field effects and pulse tests in soil samples*. Géotechnique, 53, n. 3, pp. 337-345.

ARROYO M., MUIR WOOD D., GREENING P.D., MEDINA L., RIO J. (2006) – *Effects of sample size on bender-based axial G_o measurements*. Géotechnique, 56, n. 1, pp. 39-52.

BELLOTTI R., JAMIOLKOWSKI M., LO PRESTI D.C.F., O'NEILL D.A. (1996) – *Anisotropy of small strain stiffness in Ticino sand*. Géotechnique, 46, n. 1, pp. 115-131.

BRIGNOLI E.G.M., GOTTI M. (1992) – *Misure della velocità di onde elastiche di taglio in laboratorio con l'impiego di trasduttori piezoelettrici*. Rivista Italiana di Geotecnica, 26, n. 1, pp. 5-16.

DEWOOLKAR M., GODDERY T., STURE S., KO H.Y. (1997) – *Multiaxial cubical cell apparatus for cohesive and cohesionless soils: Description and users manual*. Department of Civil, Environmental and Architectural Engineering, University of Colorado, Boulder.

DYVIK R., MADSHUS C. (1985) – *Lab measurements of G_{max} using bender elements*. Advances in the art of testing soils under cyclic conditions. (Ed. Khosla), ASCE, New York, pp. 186-196.

FIORAVANTE V. (2000) – *Anisotropy of small strain stiffness of Ticino and Kenya sands from seismic wave propagation measured in triaxial testing*. Soils and Foundations, 40, 4, pp. 129-142.

GAJO A., BIGONI D., MUIR WOOD D. (2004) – *Multiple shear band development and related instabilities in granular materials*. Journal of the Mechanics and Physics of Solids, 52, pp. 2683-2724.

GRAHAM J., HOULSBY G.T. (1983) – *Anisotropic elasticity of a natural clay*. Géotechnique, 33, n. 2, pp. 165-180.

GREENING P.D., NASH D.F.T. (2004) – *Frequency domain determination of G_0 using bender elements*. Geotechnical Testing Journal, 27, 3, pp. 288-294.

HOQUE E., TATSUOKA F. (2004) – *Effects of stress ratio on small-strain stiffness during triaxial shearing*. Géotechnique, 54, n. 7, pp. 429-439.

JOVIČIĆ V., COOP M.R., SIMIĆ M. (1996) – *Objective criteria for determining G_{max} from bender element tests*. Géotechnique, 46, n. 2, pp. 357-362.

KO H.Y., SCOTT R.F. (1967) – *A new soil testing apparatus*. Géotechnique, 17, n. 1, pp. 40-57.

KUWANO R., CONNOLLY T.M., JARDINE R.J. (2000) – *Anisotropic stiffness measurements in a stress-path triaxial cell*. Geotechnical Testing Journal, 23, 2, pp. 141-157.

KUWANO R., JARDINE R.J. *(2002)* – *On the application of cross-anisotropic elasticity to granular materials at very small strains*. Géotechnique, 52, n. 10, pp. 727-749.

LEE J.N.K. (1993) – *Experimental study of body wave velocities in sand under anisotropic consolidations*. PhD Thesis, University of Texas at Austin.

LEWIS M.D. (1990) – *A laboratory study of the effect of stress state of the elastic moduli of sand*. PhD Thesis, University of Texas at Austin.

LINGS M.L. (2001) – *Drained and undrained anisotropic elastic stiffness parameters*. Géotechnique, 51, n. 6, pp. 555-565.

LINGS M.L., GREENING P.D. (2001) – *A novel bender/extender element for soil testing*. Géotechnique, 51, n. 8, pp. 713-717.

MIURA S., TOKI S. (1982) – *A sample preparation method and its effect on static and cyclic deformation-strength properties of sand*. Soils and Foundations, 22, 1, pp. 61-77.

MUIR WOOD D. (2004) – *Geotechnical modelling*. E. and F.N. Spon.

MUIR WOOD D., JAVAHERI H., SADEK T., DIHORU L., LINGS M.L. (2006) – *Deviatoric stress-response envelopes from multiaxial tests on sand*. Proc. Tatsuoka Symposium, Rome (Eds. H. Ling and L. Callisto) (to appear).

MUIR WOOD D., LINGS. M.L, NASH D.F.T., GAJO A. (2001) – *Anisotropy of soils: laboratory measurements and constitutive implementation*. Proc. 15th ICS-

MGE, Istanbul (Ed. Publications Committee of the 15th ICSMGE) Balkema 1, pp. 321-324.

PENNINGTON D.S., NASH D.F.T., LINGS M.L. (1997) – *Anisotropy of G_o shear stiffness in Gault clay*. Géotechnique, 47, n. 3, pp. 391-398.

PENNINGTON D.S., NASH D.F.T., LINGS M.L. (2001) – *Horizontally mounted bender elements for measuring anisotropic shear moduli in triaxial clay specimens*. Geotechnical Testing Journal, 24, 2, pp. 133-144.

POROVIC E. (1995) – *Investigations of soil behaviour using a resonant-column torsional-shear hollow cylinder apparatus.* PhD Thesis, Imperial College, University of London.

ROESLER S.K. (1979) – *Anisotropic shear modulus due to stress anisotropy*. Journal of Geotechnical Engineering Div., ASCE 105, GT7, pp. 871-880.

SADEK T. (2006) – *The multiaxial behaviour and elastic stiffness of Hostun sand.* PhD Thesis, University of Bristol.

SADEK T., LINGS M.L., DIHORU L., MUIR WOOD D. (2007) – *Anisotropic stiffness of Hostun sand*. Numerical models in geomechanics (NUMOG X: Rhodes) (Eds. G.N. Pande, S. Pietruszczak) Taylor & Francis Group, London, pp. 147-152.

SOMFAI E., ROUX J., N., SNOEIJER J.H., VAN HECKE., VAN SAARLOOS W. (2005) – *Elastic wave propagation in confined granular systems*. Physical Review Letters, E72, 021301.

STOKOE K.H., HWANG S.K., LEE J.N.K., ANDRUS R.D. (1995) – *Effects of various parameters on the stiffness and damping of soils at small to medium strains*. Proceedings of the Int. Symposium on Pre-failure Deformation of Geomaterials. Shibuya, (Eds. Mitachi and Mura), Hokkaido, Saporo 1, pp. 785-815.

STOKOE K.H., LEE J.N.K., LEE S.H.H. (1991) – *Characterization of soil in calibration chamber with seismic waves*. Proceedings of the 1st Int. Symposium on Calibration chamber Testing. (Eds. An-Bin Huang), Elsevier, New York, pp. 363-376.

STONELEY R. (1949) – *The seismological implications of aeolotropy in continental structure*. Monthly Notices, R. Astron. Soc., Geophysical Supplement, 5, pp. 343-353.

VIGGIANI G., ATKINSON J.H. (1995) – *Interpretation of bender element tests*. Géotechnique, 45, n. 1, pp. 149-154.

WHITE J.E. (1983) – *Underground sound application of seismic waves.* Elsevier, Amsterdam.

ZHANG L., THORNTON C. (2006) – *Probing the mechanical response of granular material in general 3D stress space*. Geomechanics and Geotechnics of Particulate Media (Eds. M. Hyodo, H. Murata and Y. Nakata), Taylor & Francis Group, London, ISBN 0-415-41097-5, pp. 199-203.

Trasmissione ondosa nella sabbia di Hostun: esperimenti multiassiali

Sommario

Le tecniche di indagine geofisica in laboratorio con l'utilizzo di onde trasmesse da materiali piezoceramici sono diventate molto popolari al fine di stimare la rigidezza dei terreni a un livello deformativo molto basso. Elementi piezoceramici del tipo Bender/Extender sono stati installati in una cella cubica multiassiale che è stata utilizzata per lo studio della rigidezza multiassiale della sabbia di Hostun. Gli elementi piezoceramici possono essere utilizzati per definire le caratteristiche di trasmissione di onde di taglio e di compressione sia perpendicolarmente da un lato all'altro della cella, sia diagonalmente da un lato al suo adiacente e quindi permettono di valutare gli elementi della matrice di rigidezza della sabbia in condizioni di anisotropia trasversale. Viene inoltre presentata una valutazione dell'evoluzione del grado di anisotropia elastica in condizioni di sforzo assial-simmetriche.